HHS Public Access

Author manuscript

J Am Chem Soc. Author manuscript; available in PMC 2020 March 13.

Published in final edited form as:

J Am Chem Soc. 2019 March 13; 141(10): 4264–4272. doi:10.1021/jacs.8b08488.

Drastically reduced ion mobility in a nanopore due to enhanced pairing and collisions between dehydrated ions

Jian Ma[1,+], **Kun Li**[1,+], **Zhongwu Li**[1], **Yinghua Qiu**[1], **Wei Si**[1], **Yanyan Ge**[1], **Jingjie Sha**[1], **Lei Liu**[1], **Xiao Xie**[2], **Hong Yi**[1], **Zhonghua Ni**[1], **Deyu Li**[3,*], **Yunfei Chen**[1,*]

[1]Jiangsu Key Laboratory for Design and manufacture of Micro-Nano Biomedical Instruments, School of Mechanical Engineering, Southeast University, Nanjing 211189, China

[2]China Education Council Key Laboratory of MEMS, Southeast University, Nanjing 210096, China

[3]Department of Mechanical Engineering, Vanderbilt University, Nashville, TN, 37235-1592, USA

Abstract

Ion transport through nanopores is a process of fundamental significance in nature and in engineering practice. Over the past decade, it has been found that the ion conductivity in nanopores could be drastically enhanced and different mechanisms have been proposed to explain this observation. To date, most reported studies have been carried out with relatively dilute electrolytes while ion transport in nanopores under high electrolyte concentrations (>1 M) has been rarely explored. Through systematic experimental and atomistic simulation studies with NaCl solutions, here we show that at high electrolyte concentrations, ion mobility in small nanopores could be significantly reduced from the corresponding bulk value. Subsequent molecular dynamics studies indicate that in addition to the low mobility of surface-bound ions in the Stern layer, enhanced pairing and collisions between partially dehydrated ions of opposite charges also make important contributions to the reduced ion mobility. Furthermore, we show that the extent of mobility reduction depends on the association constant between cations and anions in different electrolytes with a more drastic reduction for a larger association constant.

Graphical Abstract

[*]Corresponding Authors: deyu.li@vanderbilt.edu, yunfeichen@seu.edu.cn.

[+]Author Contributions: Jian Ma and Kun Li contribute equally to this work. All authors have given approval to the final version of the manuscript.

Supporting Information

Detailed description of the nanopore fabrication and characterization, ion conductance measurement, theoretical model for extracting ion mobility, molecular dynamics simulation model and videos of ion transport are available as supporting information.

The authors declare no competing financial interest.

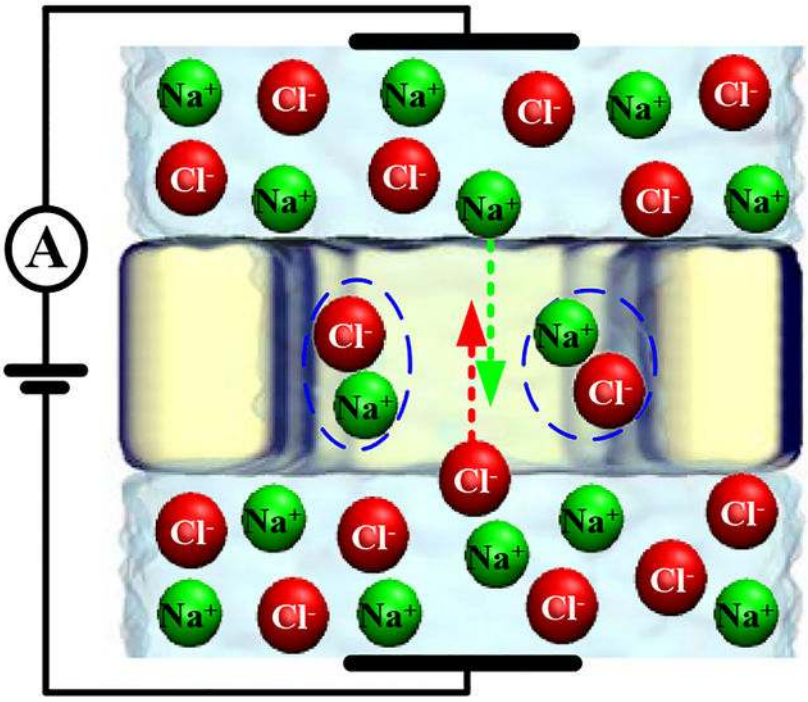

Keywords

nanopores; ion transport; ion mobility; ion pair; dehydrated ions

Introduction

Ion transport in biological and synthetic nanopores presents unique features that are critical for nanopore-based biosensing[1–4], nanofluidic chemical process[5], biomolecular separation[6–7] and electric double-layer supercapacitors[8–10]. Reducing nanopore size could not only enhance device performance but also offer opportunities for seawater desalination and sieving different ions[11–14]. It has been shown that nanopores with diameters down to 1 nm can identify single molecules[15] or significantly enhance supercapacitor capacitance[10]. With continuous decrease of the pore diameter from sub-micrometer to below 1 nm, various factors dominate ion transport through the pores, such as surface charge density[16], ion-ion interactions[17] and size effect[18]; and the current-voltage relation may display distinct linear, voltage-activated or rectified current, and different cation-selectivity profiles[16]. In fact, once the pore diameter is reduced to less than 2 nm, sub-continuum ion transport has been observed[17, 19]. Further reducing the pore diameter to sub 1 nm, ionic Coulomb blockade could occur, demonstrating a quantum-like effect dominating ion transport. These new phenomena stem from the interactions among the ions, water molecules, and nanopore surfaces that include steric repulsion, van der Waals and electrostatic interactions[20].

Among the recently-reported novel observations, one important finding is the enhanced mass transport capabilities of nanopores[21–23]. It has been shown that the flow rates of gas and water through carbon nanotubes of <2 nm diameter could be orders of magnitude higher

than those from theoretical predictions[22], which is attributed to the atomically smooth tube surface and the well-organized structure of water in the highly confined nanospace. In addition, recent experiments suggested that ion mobility in nanochannels could be higher than the corresponding bulk values[24]. Again, the well-organized water structure is thought to be responsible for the enhanced mobility because ions could experience less resistance and transport more efficiently between two ordered layers of water molecules[24].

To date, most studies of ion transport through nanopores/nanochannels have been carried out with relatively low electrolyte concentrations of ≤1 M and because the extracted ion conductivity in nanopores approaches the bulk value as the concentration increases[24–28], ion transport through nanopores at >1 M electrolyte concentrations has been thought to be bulk-like and rarely studied. However, through systematic experimental characterizations of ion conductance of a series of different diameter nanopores, here we show that the ion mobility in smaller nanopores could be remarkably lower than the corresponding bulk values at high electrolyte concentrations (>1 M). Detailed molecular dynamics studies suggest that this reduction is beyond the level that can be accounted for by the low mobility of surface-bound ions. Further examination of the ion hydration structure and transport trajectory suggests that enhanced pairing and collisions between partially dehydrated ions of opposite charges in the highly confined nanopores make more significant contribution to the ion mobility reduction.

Experimental Methods

A schematic of ion transport through a nanopore is shown in Fig. 1a. Under a bias voltage, Na^+ and Cl^- are driven through the nanopore from opposite directions. Fig. 1b illustrates the nanopore fabrication process, which is based on combined focused ion beam (FIB) milling and electron beam drilling of a silicon nitride film[29–31] (Fig. S1 and Fig. S2 in the supporting information). In our studies, we prepared a series of nanopores with diameters ranging from 2.1 to 26 nm through tuning the intensity of the focused electron beam. Fig. 1c shows a transmission electron microscopy (TEM) micrograph of a 2.1 nm diameter nanopore taken in-situ post electron beam drilling. Before measuring the ion conductance, thorough cleaning of the nanopore chip was conducted with piranha to remove contaminants. The chip was then sandwiched by two polymethyl methacrylate (PMMA) reservoirs (Fig. S3) and liquid polydimethylsiloxane (PDMS) was used to tightly seal the chip between the two reservoirs. After filling the reservoirs with degassed, filtered NaCl electrolyte, Ag/AgCl electrodes were immersed from both sides of the pore and connected to a patch clamp amplifier (HEKA EPC 10 USB, HEKA Instruments) with pico-ampere sensitivity. The set-up was placed in a double faraday cage to block electrical noises from the environment.

The nanopore conductance at various electrolyte concentrations was derived from the measured I-V curves by sweeping the applied bias from −500 mV to 500 mV with a step of 100 mV and recording the corresponding ionic current at each point. All experiments were performed at ambient conditions and the measured pH of the DI water and all other salt solutions was ~5, which was conducted with a commercial pH meter (SevenCompact S210). All the I-V data were taken after the system reached steady state. For each pore, the conductance was measured with the electrolyte concentration increasing from low to high in

sequence. For each electrolyte concentration, after replacing the electrolyte in the reservoirs, a biased voltage was applied between the two reservoirs to thoroughly flush the nanopore with the new concentration electrolyte. Ionic current was recorded until it reached a stable value before the current was taken (Fig. S4).

Ion conductance was extracted through fitting the slope of the distinct linear I-V curve and ion conductivity was derived according to the following formula[11]:

$$G = \kappa\left[\frac{4L}{\pi d^2} + \frac{1}{d}\right]^{-1}. \quad (1)$$

Here G is the measured nanopore conductance; d is the nanopore diameter extracted from the TEM characterization; L is the nanopore length, which is approximately the same as the film thickness and measured with an atomic force microscope. κ is the ion conductivity inside the nanopore. We note that Eqn. (1) is the most widely adopted equation to calculate the effective ion conductivity through nanopores[11, 27, 32]. For ion transport through nanopores under low electrolyte concentration conditions, other formula have been proposed, such as a model recently reported by Lee *et al.*[25] that can account for the effects of surface conductance. Considering the high salt concentrations investigated in our work, we chose to use Eqn. (1) to get the effective ion conductivity through the nanopore first, then discuss the factors that may affect the derived conductivity values.

Results and Discussions

Fig. 2a plots the extracted ion conductivity of different diameter nanopores along with the bulk values from 0.5 to 4 M. The data indicate remarkably lower, instead of higher, ion conductivities for smaller pores. It can be seen that while for pores of larger than 8 nm diameters, the ion conductivity is the same as that of the bulk, the conductivity demonstrates a systematic trend of lower values for smaller pores at each electrolyte concentration. This observation is counter-intuitive because it is very different from the recently reported higher ion mobility at more dilute concentrations in nanopores[24]. Importantly, the result cannot be explained by the classical Wien effect[33], either. The Wien effect suggests that ion conductance increases with electric field intensity, which would lead to a higher ion conductivity in nanopores because the electrical field strength in a nanopore can be quite large, reaching over 10^7 V/m.

Ion conductivity depends on the ion concentration and ion mobility, which can be written as:

$$\kappa = (\mu_{Na^+}\bar{n}_{Na^+} + \mu_{Cl^-}\bar{n}_{Cl^-})eN_A \quad (2)$$

Here $\bar{n}_{Na^+}$ and $\bar{n}_{Cl^-}$ are the average molar concentration and μ_{Na^+} and μ_{Cl^-} are the mobility of Na^+ and Cl^-, respectively, inside a nanopore. e is the elementary charge and N_A is the Avogadro number. In formula (2), average molar concentration is used because the

distribution for both Na^+ and Cl^- along the radial direction in a nanopore is non-uniform due to the surface charge effects. The distribution of the ion concentration, n_{Na^+} and n_{Cl^-}, can be solved from the Grahame equations[34] for high electrolyte concentrations (>1 M). Based on the obtained ion distribution along the radial direction in a nanopore, the average molar concentrations can be derived. In addition, to verify the result from the Grahame equations, we applied COMSOL Multiphysics software to model the ion concentration distribution inside the nanopore. The obtained ion concentration profiles from these two approaches match each other very well for all four reservoir concentrations of 1, 2, 3, and 4 M (Fig.S6).

From the derived ion concentrations, we solve for the ion mobility in the nanopore according to Eqn. (2) by assuming $\mu_{Cl^-} = 1.52\,\mu_{Na^+}$ (the mobility of Cl^- and Na^+ in infinitely dilute electrolytes is 7.91×10^{-8} $m^2V^{-1}s^{-1}$ and 5.19×10^{-8} $m^2V^{-1}s^{-1}$, respectively)[24, 35]. We realize that the mobility of Cl^- and Na^+ inside the nanopore under high electrolyte concentrations could be significantly different from the value for dilute bulk solutions; however, our extensive molecular dynamics (MD) results indicate that the ratio of μ_{Cl^-}/μ_{Na^+} does not change dramatically and its value is always higher than 1.52 (Fig. S15). As such, adopting the value of 1.52 will only over-estimate the mobility of Na^+ and under-estimate the mobility reduction in nanopores.

Fig. 2b plots the derived effective Na^+ mobility as a function of the electrolyte concentration for three different diameter pores in the concentration range of 0.5 to 4 M. Consistent with the ion conductivity, the Na^+ mobility in larger nanopores (>8 nm diameter) is approximately the same as the corresponding bulk value, but it becomes significantly lower in smaller nanopores. In fact, for the 2.1 nm diameter pore, the Na^+ mobility is reduced by more than 50% from the bulk value as the reservoir electrolyte concentration increases beyond 1.5 M. We note that this significantly reduced ion mobility cannot be from the uncertainty of the measured nanopore dimension. This is because the error from TEM and AFM measurement is much smaller than the measured pore dimension. Importantly, in addition to the mobility change with the pore diameter, the mobility in both the 2.6 nm and 2.1 nm diameter nanopores decreases remarkably with the increase of the electrolyte concentration, which cannot be explained by any uncertainty of the measured pore dimension.

As to the underlying mechanisms of the reduced ion mobility, it is tempting to simply attribute it to the surface-bound ions in the Stern layer, which experience enhanced drag force from the nanopore surface and have a low mobility. However, while these ions would certainly contribute to the low mobility observed for small nanopores, the above explanation cannot fully account for the systematic trend of lower mobility for higher electrolyte concentrations for the same nanopore. This is because as the electrolyte concentration increases, the double layer thickness gets smaller and the effect of the surface-bound ions should become less significant, and hence the mobility should approach the bulk value, which is exactly opposite to our experimental observation. To further confirm that the experimental observation cannot be fully explained by the surface-bound ions, we have also tried to subtract the contribution of ions in the Stern layer by eliminating their contributions

to the ion conductivity. However, no matter how we assume the Stern layer thickness, we cannot recapture the experimentally derived ion mobility, as shown in Fig. S12. Note that when we assume a Stern layer thickness of 0.34 nm, even though the difference of the obtained mobility for all nanopores is compressed, the trend becomes non-monotonic and the mobility for mid-sized pores becomes higher than the bulk value. The trend is not consistent with the experimental result and it is very difficult to imagine how the Na^+ mobility in an 8 nm diameter pore is higher than both the bulk value and that for a 2.1 nm diameter pore.

To explore the underlying mechanisms of the reduced ion mobility inside nanopores, we conducted extensive MD simulations using the classical MD package NAMD[36–37] and visualized the results using VMD[38]. In the simulation, we constructed a system with a nanopore in-between two reservoirs (Fig. S13), which was divided into *cis* and *trans* sides by a hexagonal prism silicon nitride membrane. The SiN_x membrane has a thickness of 2.6 nm along the *z* axis and an inscribed diameter in the *x*-*y* plane of 4.8 nm. A 3.0-nm diameter nanopore was drilled in the membrane center. The total system length along the *z* direction was initially set as 15.6 nm, with periodic boundary conditions imposed at the two ends. We adopted the TIP3P model for water and designated numbers of Na^+ and Cl^- were added to the reservoirs to obtain a series of ion concentrations from 0.033 M to 4.0 M. The ions were initially randomly allocated in the water and the initial velocities were given according to the Maxwell-Boltzmann distribution. The CHARMM force field[39] was adopted to model the atomic interactions between atoms of the membrane and all other atoms.

The simulation started with an energy minimization step in which the system was first allowed for structure relaxation for 1 ns. Then the system underwent a 10 ns NPT equilibration process under 1 atmospheric pressure during which only the system size in the *z*-direction was allowed to change. The final length of the system along this dimension was then taken as the average value over the last 2 ns of the equilibration. Finally, with an external electric field applied in the *z*-direction under a canonical (NVT) ensemble, 20 ns production run was performed and the last 10 ns trajectories were used in our statistical analysis. These simulation time durations are sufficient for the statistics to achieve a converged value.

Fig. 3a shows the ion concentration profiles for 2.0 M NaCl solutions along the radial direction in a 3 nm diameter silicon nitride nanopore with a surface charge density of −0.94 e/nm^2. It can be seen that other than some peaks within ~3 Å from the negatively charged nanopore surface, the ion concentration fluctuates around an average value that is slightly lower than the bulk value (2 M). The insert is the zoom-in view of Fig. 3a at the nanopore center. Fig. 3b plots the velocity profiles of the Na^+ and Cl^- for the same case, which shows that the velocity of the absorbed Na^+ in the Stern layer near the wall is much less than that in the pore center due to the drag from the pore surface. This is consistent with the expectation that surface-bound ions have very low mobility[25], which certainly contribute to the observed lower Na^+ mobility. As a comparison, the velocity based on bulk ion mobility from the MD simulations are also shown in Fig. 3b. Interestingly, for the Cl^-, the lowest velocity is not those closest to the wall but occurs at $r = 1.25$ nm, which we will explain later. In addition, Fig. 3b also indicates that in the pore center, even though the velocity profile becomes flat,

which indicates that the drag effect from the pore surface has diminished to a negligible level, the velocities of the Na^+ and Cl^- inside the nanopore are still significantly lower than those based on bulk ion mobility from the MD simulations. In fact, the simulation results indicate that the ion velocity in the pore center decreases dramatically as the electrolyte concentration increases, as shown in Fig. 3c&d. As a comparison, the velocity based on bulk ion mobility from the MD simulations at the corresponding concentration is also shown in Fig. 3c&d. It is well-known that the ion mobility in bulk electrolyte could drop slightly as the concentration increases for high concentration electrolytes (>1 M)[33]. However, comparison of the ion velocities at different concentrations indicates that in small nanopores, the ion velocity in the pore center reduces with the electrolyte concentration at a much faster rate than that needed to account for the slight drop of bulk ion mobility with concentration. As such, these MD results strongly suggest that in addition to surface-bound ions, there are other mechanisms that render lower velocity of ions even in the pore center, which also make significant contribution to the reduced ion mobility in small nanopores.

In order to quantify the contributions to the reduced ion mobility from the surface-bound ions and the reduced mobility in the pore center, we calculated the ionic current density distribution along the radial direction as shown in Fig. 3e. The NaCl concentration in the reservoirs is 2 M and the diameter is 3 nm with a surface charge density of –0.94 e/nm^2. For comparison, we also displayed the ionic current density based on the bulk ion mobility derived from the MD simulations. The top olive dash line is the ionic current density calculated using the bulk ion mobility from the MD simulation. The orange dash line is the average ionic current density in the center of the nanopore. The ionic current difference due to the low mobility of surface-bound ions and the reduced ion mobility in the pore center are also depicted in Fig. 3e. The contributions to the reduced mobility from the surface-bound ions and the enhanced pairing and collision of dehydrated ions are labelled as S_s and S_p, respectively. More quantitative analysis indicates that compared to the corresponding bulk value, the ionic current through the nanopore drops by a total of ~62%. Specifically, the low mobility of surface-bound ions contributes ~12%, while the mechanisms responsible for the reduced ion velocity in the pore center lead to the rest ~50% reduction.

Clearly, factors other than surface-bound ions have to be taken into account to explain the experimental observation. In search of the additional mechanisms, we consider the difference between our case and the conditions for higher than bulk mobility under low electrolyte concentration cases as reported in the literature. One major disparity is that while both cations and anions exist inside the nanopores in our study, only counter-ions (usually cations) present for the low electrolyte concentration cases in the literature. As such, we examined the effects of co-ions by removing all Cl^- from the simulation system. Interestingly, this operation yielded Na^+ mobility that is significantly higher than the corresponding bulk value even though in this case, the effects of surface-bound ions still exist (as shown in Fig. 3f). This observation strongly suggests that interactions between the Na^+ and Cl^- play an important role in the reduced ion mobility in nanopores of less than 8 nm diameter. As a comparison, the bulk ion mobility from the MD simulations and bulk ion mobility calculated from the CRC handbook[40] are also shown in Fig. 3f.

In order to understand how the interactions between Na^+ and Cl^- in smaller pores lead to reduced ion mobility, we carefully examine the MD data to investigate the ion transport process. In detailed examination of the ion trajectories (Videos S1–S5), we noticed that some Na^+ and Cl^- move together, i.e, they form ion pairs. In fact, the videos in the Supporting Information even show that Na^+ can sometimes move backward, which can only be the case when it forms an ion pair with Cl^- and is pushed back by the Cl^-. In the simulation, we define an ion pair as a pair of Na^+ and Cl^- that move together as a single entity and are held together by the electrostatic force of Coulomb type acting over a short distance between the ions in the ion pair. The cutoff distance to define ion-pairs[41] is 3.2 Å in the MD simulations, which is chosen based on Eqn. (3).

$$r_{cutoff} = \sqrt{r_{\max} \times r_{\min}} = \sqrt{2.7 \times 3.8} = 3.2\text{Å} \quad (3)$$

where r_{max} is the radius of the first shell of Cl^- around Na^+ (radius of the first peak in radial distribution function, g(r)); r_{min} is the radius of the first coordination shell of Cl^- around Na^+ (radius of the first minimum after r_{max}). r_{max}=2.7 Å and r_{min}=3.8 Å according to Fig. S18. The association of ions into pairs is caused by the long-range electrostatic force among the ions of opposite charges, attenuated by the solvent permittivity[42]. Ion pairs have much lower mobility because they experience much reduced electrostatic force from the external electrical field and transport through the nanopore in a manner of diffusive random walk instead of following a rather straight path of individual ions. Ion pairs also exist in bulk electrolyte[42–43] at high concentrations. As such, we compare the probability of ion pair formation in a 3 nm diameter pore and that in bulk electrolyte under the same electrolyte concentration.

Fig. 4a depicts the density of ion pairs formed inside a nanopore and in the bulk *versus* the electrolyte concentration, which clearly indicates higher ion pair concentrations inside the nanopore. This can also be seen from Fig. 4b, which shows the radial distribution function (RDF) of Cl^- around Na^+ in the 3 nm pore from the MD simulation. Fig. 4b indicates a much enhanced first peak of Cl^- around Na^+ in the nanopore than that in bulk electrolyte, suggesting more Cl^- and Na^+ are moving together as ion pairs. We note that the trend of ion pair density agrees extremely well with the derived ion mobility shown in Fig. 2b. The ion pair density in the nanopore exceeds the bulk value quickly as the electrolyte concentration increases from 0.5 to 2 M, but the difference remains nearly the same for even higher electrolyte concentrations. In Fig. 2b, especially for the 2.1 nm pore, the Na^+ mobility quickly deviates from the bulk value in the same concentration range of 0.5 to 2 M, and then the drop rate slows down significantly. The clear correspondence between the ion pair concentration and Na^+ mobility provides a strong evidence that enhanced ion pair formation inside the nanopore plays an important role in the reduced ion mobility. All results of Fig.4 are from MD simulations in a SiN_x nanopore with 3 nm diameter and 2.6 nm length. Water box on both sides of the membrane had the length of 6.5 nm. The transmembrane bias was kept at 5.8 V.

Now we consider why more ion pairs are formed in nanopores. It has been reported that ion dehydration could occur in nanometer diameter pores[18, 44]; and therefore, we solve for the

RDF of water molecules around Na^+ in the bulk and that in the nanopore. Fig. 4c presents the RDFs for the case with 2 M NaCl solution in the reservoir, which indicates a strong deviation of the RDFs in the nanopore from the corresponding bulk case. Similar results have been obtained for water molecules around Cl^- (Fig. S19). The dehydration of ions impairs the shielding effects of water molecules and enhances the interactions between Na^+ and Cl^-, which leads to higher ion pair density inside nanopores. It is also important to note that even when the distance between the partially dehydrated cations and anions is larger than that required for ion pair formation, the interactions between these ions are still stronger than those among fully hydrated ions in bulk solutions.

Ion dehydration when translocating nanopores has been reported in literature; however, the reported studies are mainly associated with hydrophobic pores of diameters less than 2.8 nm and the dehydration is attributed to steric effect[44]. For hydrophilic nanopores made of SiN_x with diameter larger than 2.1 nm, both Na^+ and Cl^- can translocate the pore with minimal steric repulsion from the nanopore surface. Now one might argue that the reduced first peak in the RDF of water molecules around Na^+ is due to that in the nanopore, more Na^+ in the Stern layer directly contact the nanopore surface without water molecules in-between. This is indeed the case as shown in Fig. S22, which shows the RDF of water molecules around Na^+ in different regions in the nanopore. The high Na^+ concentration in the Stern layer (12.5 Å < r < 15 Å) leads to a much reduced first peak. However, the first peak in the RDF of water molecules in the region of 10 Å < r < 12.5 Å is also lower than that in the bulk, indicating that ions in this region is also dehydrated, and in fact, this is the region most ion pairs form. This is because in the Stern layer, few Cl^- are available to form ion pairs with Na^+, while in the diffuse layer, partially dehydrate Na^+ and Cl^- both exist and can form ion pairs. In fact, this is also the reason for that the ion velocity displays a minimum at r = 12.5 Å.

The hydration layer is partially destroyed in this near wall region because the strong electric field near the negatively charged wall helps to polarize water molecules. As such, the hydration layer of ions get partially destroyed even before ions get into the Stern layer. We note that even though ion pairs are mostly formed in the region of 10 Å < r < 12.5 Å, they can diffuse into the pore center to reduce the average ion velocity in the pore center. This can also be discerned from careful examination of the supplementary videos (Videos S1–S5), which reveal that when a Cl^- encounters a Na^+ near the nanopore surface, the chance for ion pair formation is higher than when these ions meet with each other in the nanopore center, because of the stronger attraction force between more dehydration ions in the near-wall region. The above understanding is also consistent with the report that the hydration layer around an ion inside a small nanopore is more prone to be destroyed than that in a larger pore[34]. We note that this is the reason for the definition of S_p and S_s in Fig. 3e. Since enhanced ion pairing and collisions also occur in the near wall region, in our calculation of S_p, we count the ionic current density difference across the entire nanopore cross-section.

To demonstrate the effect of enhanced pairing and collisions between partially dehydrated ions more straightforwardly, Fig. 4d plots the histogram of the Na^+ translocation time distributions and fittings using the first-passage probability density function[45]. It can be easily seen from Fig. 4d that the dwell time of Na^+ inside the nanopore for the 4 M case is

much longer than that for the 0.5 M case because of more ion pairs and enhanced interactions between the Na^+ and Cl^-. This is also evident from the supporting videos, which suggests that with the increase of the electrolyte concentrations from 0.05 M to 4 M, the trajectory of ions translocating a nanopore changes from an almost straight line to a zigzag path. In fact, without Cl^- in the nanopore, the Na^+ travels along a straight trajectory, as shown in video S4. However, with Cl^- in the pore, pairing and collisions between Na^+ and Cl^- lead to highly diffuse transport, as can be seen from video S5. Finally, we point out that as the nanopore diameter increases, the hydration layer around both Na^+ and Cl^- away from the pore surface is less distorted without the assistance of negatively charged wall and the ion mobility approaches the bulk value.

One more factor to consider is the effect of external electrical field applied across the nanopore. In our MD simulation, we applied rather strong electrical field (on the order of ~10^9 V/m) to achieve convergent ion velocity within a reasonable amount of simulation time. The strong external electrical field could help to polarize the water molecules inside the nanopore (as shown by the probability distribution of the dipole orientation for water molecules inside SiN_x nanopore for different bias voltage in Fig. S20), which might also facilitate ion dehydration. It is important to note that in our experimental setup, the electrical field intensity inside the nanopore is on the order of ~10^7 V/m. While this value far exceeds the normal values usually encountered in bulk solutions, it is still about two orders of magnitude smaller than the value in MD simulation. Therefore, it is critical to verify that ion dehydration occurs under low external electric field. Since it is possible to obtain the radial distribution function of water molecules around Na^+ under low electric field intensity using MD, as long as we do not intend to extract the ion velocity, we calculated the radial distribution function using the same MD model but without an external electric field (Fig. S21). The results clearly indicate that ion dehydration still occurs, even though the distortion is slightly weaker than that in Fig. 4c. Therefore, we can safely conclude that the mechanisms disclosed from the MD analysis could be applied to explain our experimental observation.

To further confirm the above analysis, we conducted additional experiments with other types of electrolytes, including KI, LiI, and HCl, with different association tendencies for cations and anions to form ion pairs. The likelihood for ions in each electrolyte to form ion pairs can be measured by the association constant, K_A, defined as $K_A = [CA]/([C^+][A^-])$ for the ionization equilibrium $C^+ + A^- \rightleftharpoons CA$ for salt CA. Here C^+ stands for the dissociated cations, A^- for the dissociated anions, and CA for the paired ions, while square brackets denote molar concentration of each species. If ion pairing does play a significant role in reducing the ion mobility inside the nanopore, then we can expect that for a lower association constant, i.e., it is more difficult for ions to form ion pairs, the difference between the ion mobility in the nanopore and in the bulk will become smaller.

These additional measurements were done with a nanopore of 2.8 nm diameter and 10 nm length and the measurements were conducted in the same fashion as that for the NaCl solution with the electrolyte concentration in the reservoirs ramping from 0.1 M to 4 M. The derived trend of conductivity *versus* concentration for each type of electrolyte is depicted in Fig. S5, together with the bulk conductivity[40, 46] for comparison. The results show that as

the electrolyte concentration increases beyond 1 M, the ion conductivity through the nanopore for the KI, NaCl, and LiI electrolyte is lower than the corresponding bulk values, while the conductivity of the HCl is approximately the same as that of bulk in the entire measurement concentration range.

To further solve for the mobility of cations in the nanopore for these electrolytes, we follow the same approach as we did for the NaCl electrolyte based on Eq. (2) for different electrolytes. Again, we assume the mobility ratios of I:K, I:Li and Cl:H as those for infinite dilution solutions in the calculation, with respective values taken as 1, 1.985 and 0.218[40]. In addition, the average concentrations of cations and anions are calculated using the Grahame equations, similar to what we have done for NaCl. The extracted cation mobility *versus* concentration for different electrolytes is plotted in Fig. S8, together with the cation ion mobility in bulk electrolyte for comparison.

To disclose the relation between cation mobility reduction inside the nanopore and the association constant, we plot the mobility ratio, $\mu_{\text{nanopore}}/\mu_{\text{bulk}}$, *versus* $\ln K_A$ for all four different electrolytes at 2 M concentration, as shown in Fig. 5a, which demonstrates a systematic trend of more significant mobility reduction for higher K_A, consistent with our expectation. The K_A value reduces in the sequence of KI, NaCl and LiI with its logarithm values as −0.8, −1 and −5.7, respectively[47], indicating that as it becomes more difficult for ion pairs to form, the reduction of cation mobility inside the nanopore tends to be less significant. HCl is a strong acid and is considered to completely dissociate in water with $\ln K_A = -21.4$[48]. Therefore, there is essentially no H^+ and Cl^- ion pair in HCl either in the nanopore or bulk electrolyte, and we have $\mu_{\text{nanopore}}/\mu_{\text{bulk}}=1$ for HCl.

As mentioned previously, ion conductivity in nanopores/nanochannels filled with low concentration electrolytes has been reported in quite a few reports;[24, 26, 49–50] and therefore, it is important for us to conduct the same measurements and verify that we can obtain similar results, which could provide important confirmation of the solidness of our high electrolyte concentration data. Fig. 5b plots the ion conductivity at low electrolyte concentrations, which shows surface charge controlled transport, consistent with those reported in the literature. These results provide additional confidence in our results for higher electrolyte concentrations as the experiment is done continuously from low to high concentrations. In addition, with our new understanding of the reduced ion mobility in small nanopores at high electrolyte concentrations showing the key roles played by enhanced ion pairing and electrostatic interactions between cations and anions, we believe that lack of these effects in more dilute concentration cases should be a factor for the enhanced ion mobility in nanochannels first disclosed by Duan et al.[24] We note that importantly, there could be other factors that also contribute to the enhanced ion mobility, such as the more organized water molecule arrangement allowing for low resistance ion paths through nanopores/nanochannels, as suggested by Duan et al.[24]

One more factor that could be important is the nanopore surface roughness. The inner surface of the nanopore should not be atomically smooth as that for carbon nanotubes; however, the reduced ion mobility at high electrolyte concentrations should not be attributed to the surface roughness because the same phenomenon occurs in molecular dynamics

simulation with smooth nanopore surface. In fact, the consistency between the experimental data and MD results strongly suggests that factors that are not considered in the MD simulation might not play a critical role in the observed reduced ion mobility. It is also worth noting that we observed enhanced ion mobility at low electrolyte concentrations, which is consistent with that reported in the literature.

Conclusions

In summary, we studied ion transport through nanopores over a whole spectrum of electrolyte concentration range spanning from 10^{-7} M all the way up to 4 M. Interestingly, it is found that contrary to the common expectation, ion transport through nanopores could also significantly deviate from bulk behavior at high electrolyte concentrations with much reduced ion mobility. Detailed MD studies indicate that the lower than bulk ion mobility observed at high electrolyte concentrations is due to the combined effects of the low mobility of surface-bound ions and enhanced pairing and collisions between partially dehydrated ions of opposite charges. The study also provides insight into the higher than bulk ion mobility in nanochannels for dilute (<0.1 M) electrolytes. As such, the ion mobility in nanopore/channels continuously decreases as the electrolyte concentration increases. The new, more complete physical picture of ion transport through nanopores could provide important insights into designing novel nanofluidic devices and high performance supercapacitors.

Supplementary Material

Refer to Web version on PubMed Central for supplementary material.

Acknowledgment

The authors thank the Natural Science Foundation of China (Grants No.51435003, No. 51302037, No.51375092, No.51705075 and No. 51675101), and the Jiangsu Province Nature Science Foundation (Grant No. BK2009292) for financial support. D.L. appreciates the financial support from the U.S. National Institute of Health (1R21EY026176 and 1R01EY027729). Yunfei Chen and Kun Li also thank PanYu Chen for his constructive comments and discussions. Jian Ma also appreciates the Fundamental Research Funds for the Central Universities.

References

1. Kasianowicz JJ; Brandin E; Branton D; Deamer DW, Characterization of individual polynucleotide molecules using a membrane channel. Proc. Natl. Acad. Sci. U.S.A 1996, 93 (24), 13770–13773. [PubMed: 8943010]
2. Healy K; Schiedt B; Morrison AP, Solid-state nanopore technologies for nanopore-based DNA analysis. Nanomedicine 2007, 2 (6), 875–897. [PubMed: 18095852]
3. Haque F; Li JH; Wu HC; Liang XJ; Guo PX, Solid-state and biological nanopore for real-time sensing of single chemical and sequencing of DNA. Nano Today 2013, 8 (1), 56–74. [PubMed: 23504223]
4. Venkatesan BM; Bashir R, Nanopore sensors for nucleic acid analysis. Nat. Nanotechnol 2011, 6 (10), 615–624. [PubMed: 21926981]
5. Tamaki E; Hibara A; Kim HB; Tokeshi M; Kitamori T, Pressure-driven flow control system for nanofluidic chemical process. J. Chromatogr., A 2006, 1137 (2), 256–262. [PubMed: 17129585]
6. Jirage KB; Hulteen JC; Martin CR, Nanotubule-based molecular-filtration membranes. Science 1997, 278 (5338), 655–658.

7. Han J; Craighead HG, Separation of long DNA molecules in a microfabricated entropic trap array. Science 2000, 288 (5468), 1026–1029. [PubMed: 10807568]
8. Lu XF; Li GR; Tong YX, A review of negative electrode materials for electrochemical supercapacitors. Sci. China. Technol. Sc 2015, 58 (11), 1799–1808.
9. Wang GP; Zhang L; Zhang JJ, A review of electrode materials for electrochemical supercapacitors. Chem. Soc. Rev 2012, 41 (2), 797–828. [PubMed: 21779609]
10. Chmiola J; Yushin G; Gogotsi Y; Portet C; Simon P; Taberna PL, Anomalous increase in carbon capacitance at pore sizes less than 1 nanometer. Science 2006, 313 (5794), 1760–1763. [PubMed: 16917025]
11. Wanunu M; Dadosh T; Ray V; Jin JM; McReynolds L; Drndic M, Rapid electronic detection of probe-specific microRNAs using thin nanopore sensors. Nat. Nanotechnol 2010, 5 (11), 807–814. [PubMed: 20972437]
12. Heiranian M; Farimani AB; Aluru NR, Water desalination with a single-layer MoS2 nanopore. Nat. Commun 2015, 6, 8616. [PubMed: 26465062]
13. Celebi K; Buchheim J; Wyss RM; Droudian A; Gasser P; Shorubalko I; Kye JI; Lee C; Park HG, Ultimate permeation across atomically thin porous graphene. Science 2014, 344 (6181), 289–92. [PubMed: 24744372]
14. Choi W; Ulissi ZW; Shimizu SF; Bellisario DO; Ellison MD; Strano MS, Diameter-dependent ion transport through the interior of isolated single-walled carbon nanotubes. Nat. Commun 2013, 4, 2397. [PubMed: 24025921]
15. Lindsay S, The promises and challenges of solid-state sequencing. Nat. Nanotechnol 2016, 11 (2), 109–111. [PubMed: 26839253]
16. Jain T; Rasera BC; Guerrero RJ; Boutilier MS; O'Hern SC; Idrobo JC; Karnik R, Heterogeneous sub-continuum ionic transport in statistically isolated graphene nanopores. Nat. Nanotechnol 2015, 10 (12), 1053–1057. [PubMed: 26436566]
17. Feng J; Ke L; Graf M; Dumcenco D; Kis A; Ventra MD; Radenovic A, Observation of ionic Coulomb blockade in nanopores. Nat. Mater 2016, 15 (8), 850. [PubMed: 27019385]
18. Zwolak M; Lagerqvist J; Di Ventra M, Quantized ionic conductance in nanopores. Phys. Rev. Lett 2009, 103 (12), 128102. [PubMed: 19792463]
19. Choi W; Ulissi ZW; Shimizu SFE; Bellisario DO; Ellison MD; Strano MS, Diameter-dependent ion transport through the interior of isolated single-walled carbon nanotubes. Nat. Commun 2013, 4 (4), 2397. [PubMed: 24025921]
20. Sparreboom W; van den Berg A; Eijkel JCT, Principles and applications of nanofluidic transport. Nat. Nanotechnol 2009, 4 (11), 713–720. [PubMed: 19898499]
21. Dellago C; Naor MM; Hummer G, Proton transport through water-filled carbon nanotubes. Phys. Rev. Lett 2003, 90 (10), 105902. [PubMed: 12689010]
22. Holt JK; Park HG; Wang YM; Stadermann M; Artyukhin AB; Grigoropoulos CP; Noy A; Bakajin O, Fast mass transport through sub-2-nanometer carbon nanotubes. Science 2006, 312 (5776), 1034–1037. [PubMed: 16709781]
23. Tunuguntla RH; Allen FI; Kim K; Belliveau A; Noy A, Ultrafast proton transport in sub-1-nm diameter carbon nanotube porins. Nat. Nanotechnol 2016, 11, 639. [PubMed: 27043198]
24. Duan CH; Majumdar A, Anomalous ion transport in 2-nm hydrophilic nanochannels. Nat. Nanotechnol 2010, 5 (12), 848–852. [PubMed: 21113159]
25. Lee C; Joly L; Siria A; Biance AL; Fulcrand R; Bocquet L, Large Apparent Electric Size of Solid-State Nanopores Due to Spatially Extended Surface Conduction. Nano Lett 2012, 12 (8), 4037–4044. [PubMed: 22746297]
26. Stein D; Kruithof M; Dekker C, Surface-charge-governed ion transport in nanofluidic channels. Phys. Rev. Lett 2004, 93 (3), 035901. [PubMed: 15323836]
27. Smeets RMM; Keyser UF; Krapf D; Wu MY; Dekker NH; Dekker C, Salt dependence of ion transport and DNA translocation through solid-state nanopores. Nano Lett 2006, 6 (1), 89–95. [PubMed: 16402793]
28. Fologea D; Uplinger J; Thomas B; McNabb DS; Li JL, Slowing DNA translocation in a solid-state nanopore. Nano Lett 2005, 5 (9), 1734–1737. [PubMed: 16159215]

29. Ho C; Qiao R; Heng JB; Chatterjee A; Timp RJ; Aluru NR; Timp G, Electrolytic transport through a synthetic nanometer-diameter pore. Proc. Natl. Acad. Sci. U. S. A 2005, 102 (30), 10445–10450. [PubMed: 16020525]
30. Ma J; Qiu Y; Yuan Z; Zhang Y; Sha J; Liu L; Sun L; Ni Z; Yi H; Li D, Detection of short single-strand DNA homopolymers with ultrathin S i 3 N 4 nanopores. Phys. Rev. E 2015, 92 (2), 022719.
31. Marshall MM; Yang J; Hall AR, Direct and transmission milling of suspended silicon nitride membranes with a focused helium ion beam. Scanning 2012, 34 (2), 101–106. [PubMed: 22331671]
32. Kowalczyk SW; Grosberg AY; Rabin Y; Dekker C, Modeling the conductance and DNA blockade of solid-state nanopores. Nanotechnology 2011, 22 (31),345101. [PubMed: 21795772]
33. Wright MR, An Introduction to Aqueous Electrolyte Solutions John Wiley & Sons: Hoboken, 2007.
34. Israelachvili JN, Intermolecular and Surface Forces, 3rd ed.; Academic Press: Waltham, MA, 2011.
35. Baldessari F, Electrokinetics in nanochannels - Part I. Electric double layer overlap and channel-to-well equilibrium. J. Colloid Interface Sci 2008, 325 (2), 526–538. [PubMed: 18639883]
36. Aksimentiev A; Schulten K, Imaging alpha-hemolysin with molecular dynamics: ionic conductance, osmotic permeability, and the electrostatic potential map. Biophys. J 2005, 88 (6), 3745–61. [PubMed: 15764651]
37. Phillips JC; Braun R; Wang W; Gumbart J; Tajkhorshid E; Villa E; Chipot C; Skeel RD; Kale L; Schulten K, Scalable molecular dynamics with NAMD. J. Comput. Chem 2005, 26 (16), 1781–802. [PubMed: 16222654]
38. Humphrey W; Dalke A; Schulten K, VMD: Visual molecular dynamics. J. Mol. Graph. Model 1996, 14 (1), 33–38.
39. Jorgensen WL; Maxwell DS; TiradoRives J, Development and testing of the OPLS all-atom force field on conformational energetics and properties of organic liquids. J. Am. Chem. Soc 1996, 118 (45), 11225–11236.
40. Lide DR, CRC Handbook of Chemistry and Physics, 90th ed.; CRC Press, Taylor and Francis: New York, 2009.
41. Joung IS; Cheatham III TE, Molecular dynamics simulations of the dynamic and energetic properties of alkali and halide ions using water-model-specific ion parameters. J. Phys. Chem. B 2009, 113 (40), 13279–13290. [PubMed: 19757835]
42. Marcus Y; Hefter G, Ion pairing. Chem. Rev 2006, 106 (11), 4585–621. [PubMed: 17091929]
43. Bian H; Chen H; Zhang Q; Li J; Wen X; Zhuang W; Zheng J, Cation Effects on Rotational Dynamics of Anions and Water Molecules in Alkali (Li+, Na+, K+, Cs+) Thiocyanate (SCN–) Aqueous Solutions. J. Phys. Chem. B 2013, 117 (26), 7972–7984. [PubMed: 23763605]
44. Sahu S; Di Ventra M; Zwolak M, Dehydration as a Universal Mechanism for Ion Selectivity in Graphene and Other Atomically Thin Pores. Nano Lett 2017, 17 (8), 4719–4724. [PubMed: 28678508]
45. Ling DY; Ling XS, On the distribution of DNA translocation times in solid-state nanopores: an analysis using Schrödinger's first-passage-time theory. J. Phys.: Condens. Matter 2013, 25 (37), 375102. [PubMed: 23963318]
46. Dean JA, Lange's Handbook of Chemistry, 15th ed.; MacGraw-Hill: New York, 1999.
47. Fennell CJ; Bizjak A; Vlachy V; Dill KA, Ion Pairing in Molecular Simulations of Aqueous Alkali Halide Solutions. J. Phys. Chem. B 2009, 113 (19), 6782–6791. [PubMed: 19206510]
48. Kren RM, Inorganic Energetics, an Introduction, 2nd Edition - Dasent,We. J. Am. Chem. Soc 1983, 105 (16), 5513–5514.
49. Feng JD; Graf M; Liu K; Ovchinnikov D; Dumcenco D; Heiranian M; Nandigana V; Aluru NR; Kis A; Radenovic A, Single-layer MoS2 nanopores as nanopower generators. Nature 2016, 536 (7615), 197. [PubMed: 27409806]
50. Siria A; Poncharal P; Biance AL; Fulcrand R; Blase X; Purcell ST; Bocquet L, Giant osmotic energy conversion measured in a single transmembrane boron nitride nanotube. Nature 2013, 494 (7438), 455–458. [PubMed: 23446417]

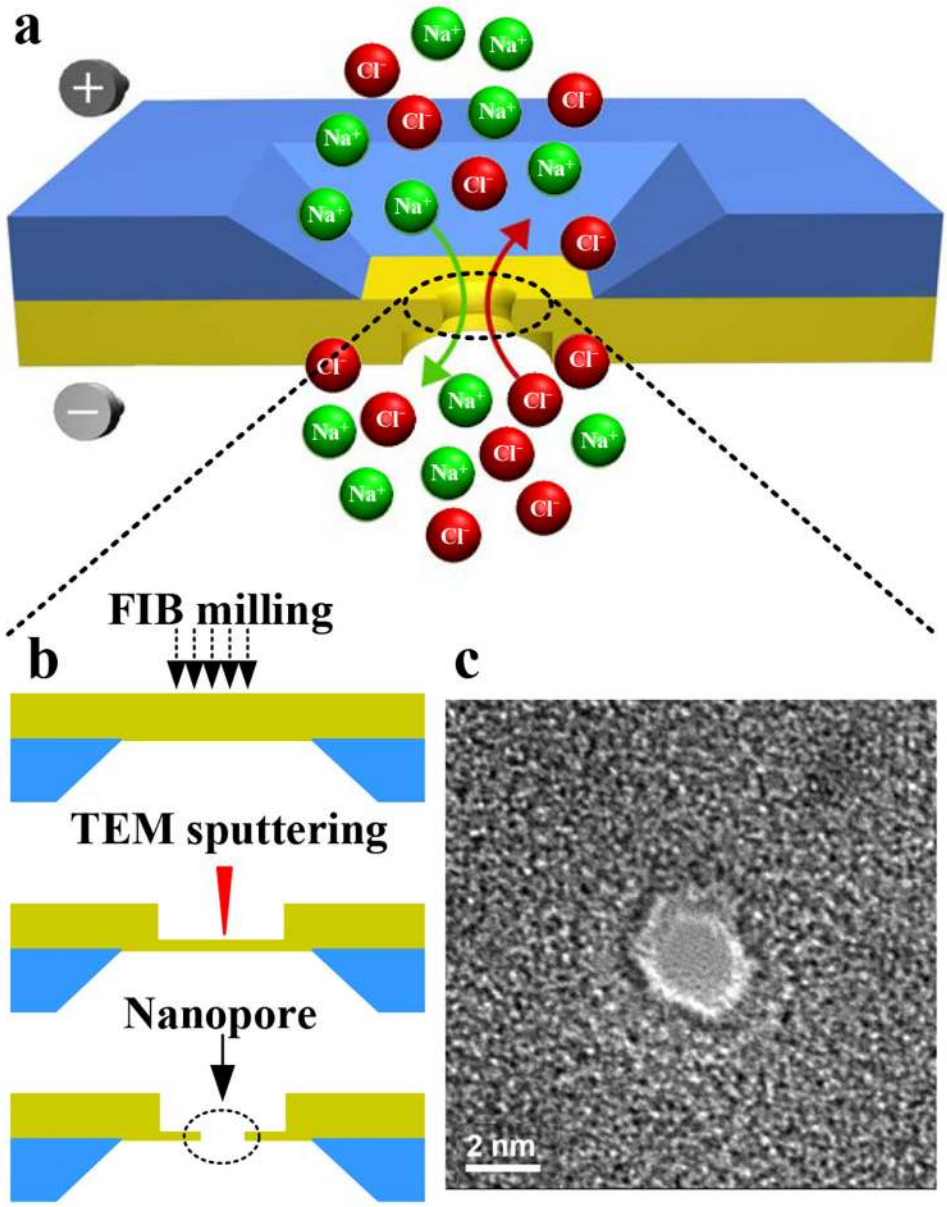

Figure 1.

Experimental setup for measuring the ion current through a nanopore. (**a**) Schematic of ion transport through a nanopore, (**b**) Nanopore fabrication process involving FIB milling of a SiN_x membrane and TEM sputtering the nanopore, and (**c**) A TEM micrograph of a nanopore of ~2.1 nm diameter.

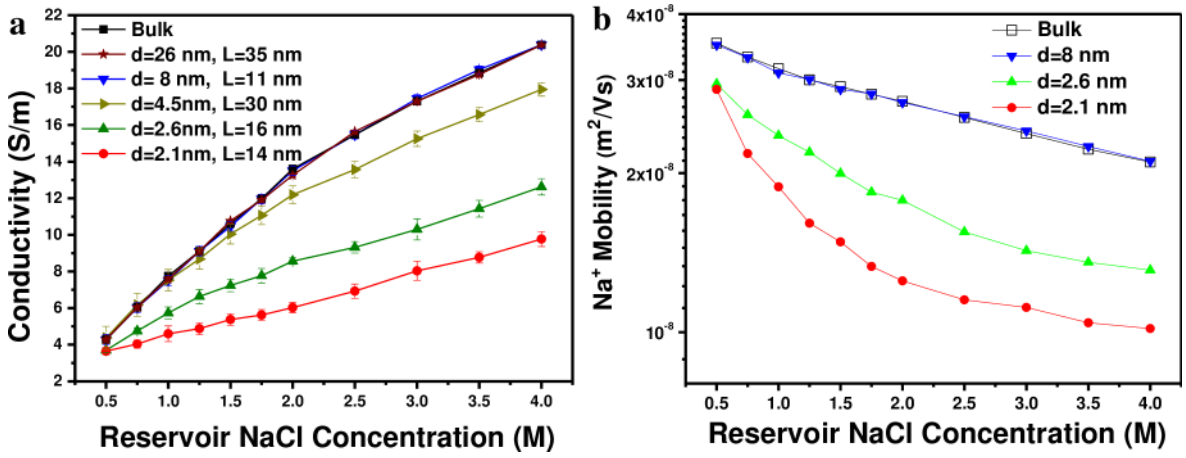

Figure 2.

(**a**) Ion conductivity of NaCl solutions with concentrations ranging from 0.5 M to 4 M. The black rectangle points stand for the ion conductivity for bulk NaCl solutions. (**b**) The mobility of Na^+ in nanopores as a function of the NaCl concentration in the reservoirs.

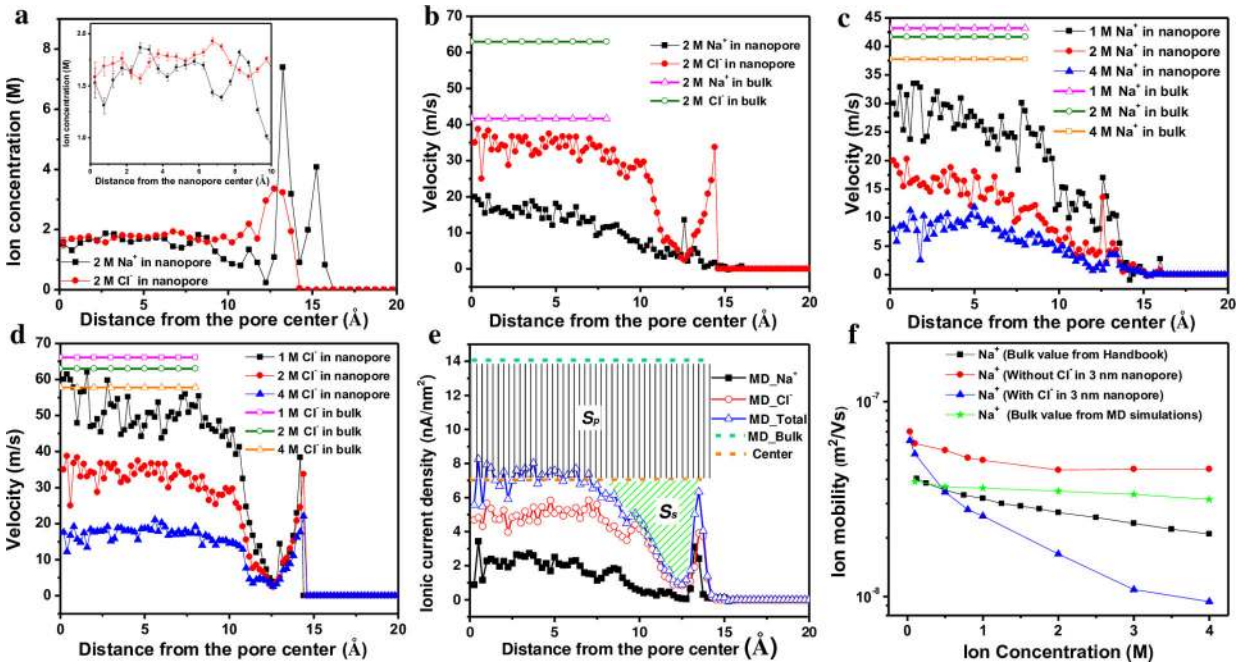

Figure 3.

Molecular dynamics results for (**a**) Ion concentration distribution and (**b**) Ion velocity distribution along the radial direction. The inset of (**a**) is a zoom-in view the ion concentrations in the center region. The velocity profiles for (**c**) Na^+ and (**d**) Cl^- for 1.0 M, 2.0 M and 4.0 M NaCl concentrations from MD simulations. (**e**) MD simulation results of the ionic current density. (**f**) The ion mobility from MD simulation of a 3 nm diameter nanopore as a function of the NaCl concentration in the reservoirs. Error bars represent standard errors and are smaller than the symbols.

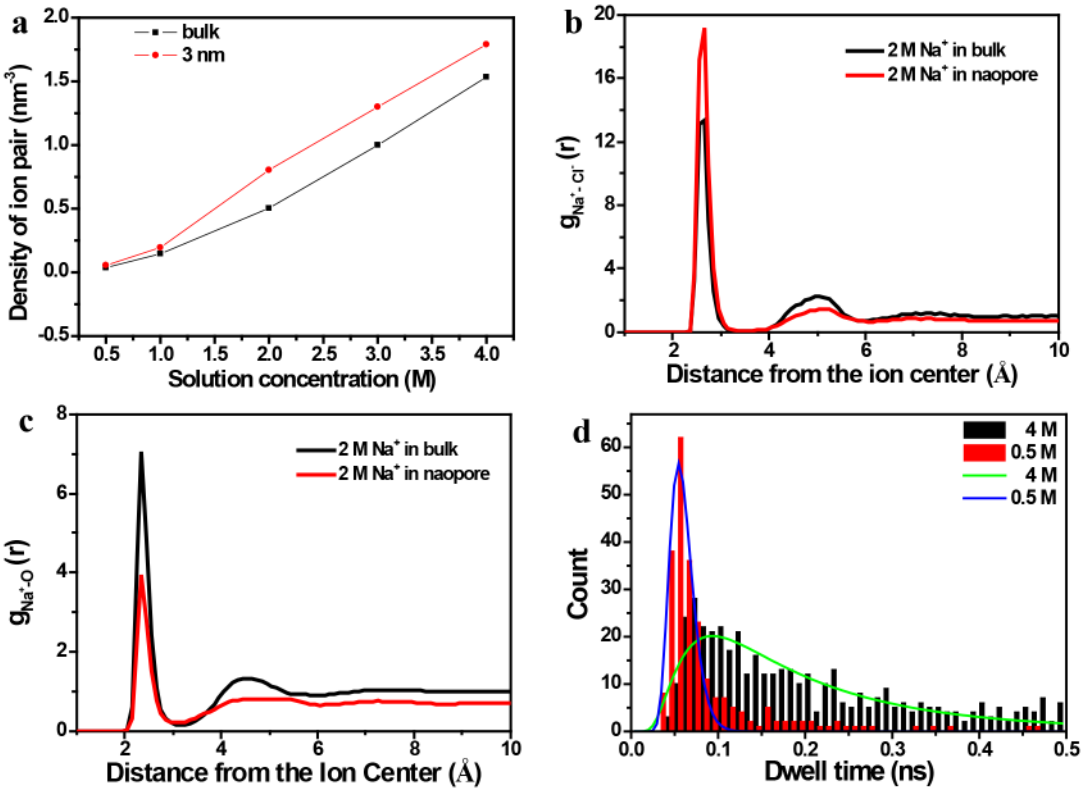

Figure 4.

(**a**) The density of the ion pairs formed in a nanopore and in the bulk versus the salt concentrations. (**b**) The radial distribution function of Cl^- around Na^+ in the bulk and in the nanopore, respectively. (**c**) The radial distribution function of water molecules around a Na^+ ion in bulk solution and inside a nanopore. (**d**) Histogram of the dwell time for Na^+ translocating through a nanopore and fittings using the first-passage probability density function. Error bars represent standard errors and are smaller than the symbols.

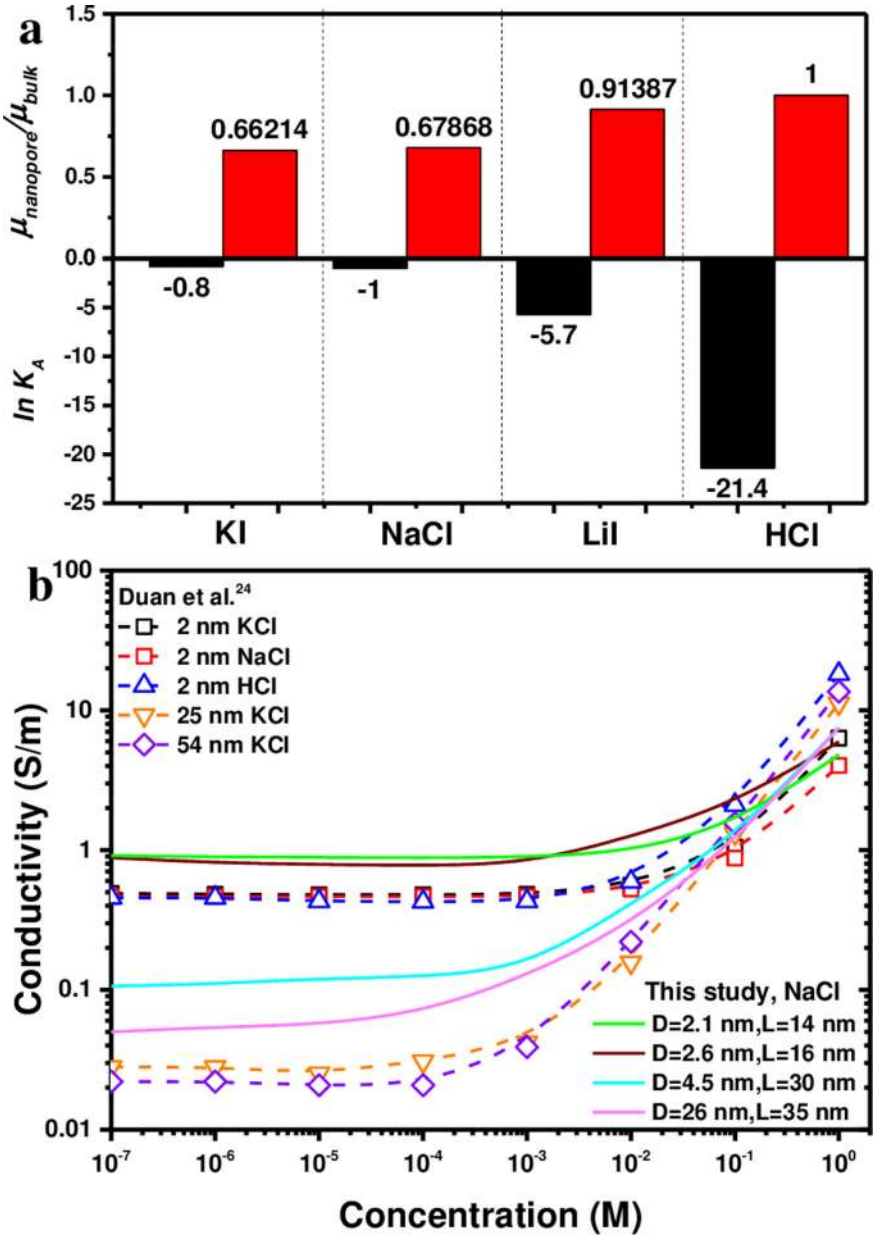

Figure 5:

(**a**) The ratio of cation mobility in the nanopore to the corresponding bulk value at 2 M concentration *versus* the association constant (K_A). (**b**) Measured ion conductivity at low concentrations in comparison with the data from Duan et al.[24]